https://doi.org/10.5194/egusphere-2022-9
Preprint. Discussion started: 1 March 2022

Technical Note: Quantifying Hazard Probability and Risk from Ensemble Projections of Downscaled Climate Variables

James P. Kossin[1], Timothy M. Hall[1], Terence R. Thompson[1]

[1]The Climate Service (an S&P Global company), 110 Corcoran St., Durham, NC, 27701, USA

Correspondence to: James P. Kossin (james.kossin@theclimateservice.com)

Abstract. Hazard metrics downscaled from climate model projections are commonly used for assessing future risk and related potential losses at local spatial scales. Quantifying changes in risk into actionable information is essential for building resilience to climate change through adaptation of existing operational assets, siting and design of future assets, identifying transition risks as well as opportunities, determining optimal paths towards net-zero carbon operations, and assessing future cost/benefit ratios for many other current and future actions. In addition to projecting the most-likely, or expected, values for a given hazard, it is important to quantify the probability distribution for that hazard at any specified time in the future. Here we describe a method to incorporate uncertainty in the downscaled hazard metrics to produce a probabilistic forecast, first for any single model, and then for a multi-model ensemble. The uncertainty for any single model represents an estimate of the natural variability of the hazard that is intrinsic to that model, while the uncertainty in the ensemble represents the natural variability of all the models as well as the spread of each model's projected most-likely value of the hazard. Loss probability can then be determined from the hazard probability via application of impact (or damage) functions that link hazard to loss. The method is first applied to a simple temperature-based hazard variable and then to a multi-climate-variable-based hazard (fluvial flood). More general application procedures are also discussed.

Plain language summary. We describe a method to incorporate uncertainty in downscaled model ensemble projections of climate hazards, and use this uncertainty to create probabilistic projections. The uncertainty comes from two distinct sources: 1) the intrinsic natural variability of each model in the ensemble and 2) the differences, or spread, among the models. Both sources of uncertainty are used to create finite mixture distributions that can be used to form hazard and loss probability for any projected time period.

1 Introduction

The need for actionable information to quantify climate-driven changes in risk at a local level is growing rapidly. The introduction of the Task Force on Climate-related Financial Disclosures (TCFD, 2017), the rapid acceptance and implementation of TCFD recommendations by over 1,500 organizations globally (TCFD, 2020), and the present support of

https://doi.org/10.5194/egusphere-2022-9
Preprint. Discussion started: 1 March 2022

over 2,600 organizations (TCFD, 2021) has created great demand for increasing organizational and corporate awareness of both the risks and the opportunities presented by a changing climate. In response to this demand, a number of climate service providers (CSP) have recently emerged (e.g., Keenan, 2019) to provide actionable information based on a variety of methods and data sources. Often this information is provided based on projections of the most-likely value of some hazard variable at some particular time, but it is also generally desirable to have a projected range of likelihoods.

In some cases, the most-likely value may be computed as the average of a number of separate model projections with a range described by the differences between the models (often referred to as "model spread"). But it is important to also incorporate the natural variability intrinsic to each model. For example, the slowly-evolving climate signal (e.g., a trend, not necessarily linear) may suggest a certain most-likely value for some hazard in some specified year in the future, but random variability and/or a naturally-occurring event (e.g., an El Niño) can push the hazard value far from that expected value in any given year. Our goal here is to incorporate the two sources of uncertainty, one from the intrinsic natural variability in each model and the other from the spread among the individual models, into a single multi-model probabilistic hazard projection. The probabilistic hazard projection can then be used to derive a probabilistic loss, or risk, projection.

2 Data

We use NASA Earth Exchange Global Daily Downscaled Climate Projections (NEX-GDDP) data (Thrasher et al. 2012). The data comprise daily measures of surface temperature and precipitation downscaled from 21 General Circulation Model runs from the Coupled Model Intercomparison Project Phase 5 (CMIP5, Taylor et al. 2012) models (the models used and other information is found in the technical note available at https://esgf.nccs.nasa.gov/esgdoc/NEX-GDDP_Tech_Note_v0.pdf). The models are run under four Representative Concentration Pathways (RCPs, Meinshausen et al. 2011) greenhouse gas emissions scenarios (RCP2.6, RCP4.5, RCP6, and RCP8.5). The NEX-GDDP data are downscaled from two of these pathways (RCP4.5 and RCP8.5) and are provided globally on a 0.25° x 0.25° grid. The data are available for the period 1950–2099.

3 Method

3.1 Hazard probability (temperature)

The methods introduced here are general and can be applied to any hazard, but for illustrative purposes, we first develop the general method based on one hazard variable and one location. The chosen hazard is Tx90p (the annual percent of days with maximum temperature warmer than the 90th percentile local baseline daily maximum temperature), which is easily derived from the NEX-GDDP daily surface temperature data. The chosen location is Palo Alto, CA, USA. The annual time series of the 21 Tx90p projections at Palo Alto, CA USA following RCP4.5 and RCP8.5 are shown in Fig. 1. For each model, we fit a 2^{nd} order (quadratic) polynomial best-fit curve to the annual projected time series (Fig. 2). We use a quadratic fit instead of a more parsimonious linear fit because RCP projections of global-mean surface temperature can be convex upwards (e.g.,

https://doi.org/10.5194/egusphere-2022-9
Preprint. Discussion started: 1 March 2022

RCP8.5) or convex downwards (e.g., RCP4.5), and fitting a linear trend would not capture this potential behavior in our RCP-based climate hazard variables.

We consider the values along the best-fit curve as a representation of that model's climate change signal for the hazard (i.e., the model's climate sensitivity). For each model we then analyze the residuals from that model's best-fit curve. We consider the residuals as a representation of the natural variability intrinsic to that model. Ideally a model's intrinsic natural variability is identified using a large ensemble of simulations from that particular model (e.g., Knutson et al. 2013), but the available downscaled data are generally derived from single model realizations. In this case, our representation of each model's intrinsic natural variability should be considered as a best estimate.

Note that there is no expectation that the intrinsic variability of any model is in phase with any other. For example, one model may produce an El Niño event in some year and a positive Pacific Decadal Oscillation (PDO) index in some decade, and another model may produce these events in some other year and decade. In this way, the variability found in an ensemble of model time series has little physical relevance and represents only a quasi-random addition of different phases of variability among the models. That is, an ensemble of raw model time series can be used to estimate the slowly-evolving climate change signal, and the spread of the model climate change signals provides some measure of uncertainty, but the actual variability around that ensemble signal has little meaning. In order to capture the natural variability intrinsic among all the models, the variability of each individual model should be computed separately.

For each model, the residuals from the climate signal (i.e., the best-fit curve) are fit to a parametric distribution. The parametric distribution should be chosen based on the distribution of the residuals for that particular hazard variable. This is discussed further in Appendix A. For any projected time t_p, and any model m_i, the probability density function (PDF) of hazard x can be described by $f(x, t_p, m_i)$. For temperature-based variables, such as Tx90p, the residuals are typically normal, and the 2-parameter Gaussian distribution is appropriate:

$$f(x, t_p, m_i) = \frac{1}{\sigma(m_i)\sqrt{2\pi}} e^{-\frac{1}{2}\left(\frac{x-\mu(t_p,m_i)}{\sigma(m_i)}\right)^2} \quad (1)$$

where $\mu(t_p, m_i)$ is the value along the quadratic best-fit curve for model m_i at time t_p, and $\sigma(m_i)$ is the standard deviation of the residuals for model m_i. Note that when an individual modeled hazard time series is decomposed into its climate change signal and its intrinsic variability about that signal, the climate signal (e.g., the best-fit curve) comprises a time series while the variability is a fixed scalar value. For normally distributed residuals, this is simply the variance or standard deviation of the residuals. The assumption that the variance of the NEX-GDDP downscaled hazard variables is stationary under RCP warming scenarios is supported in Appendix B.

https://doi.org/10.5194/egusphere-2022-9
Preprint. Discussion started: 1 March 2022

Some hazard variables have a finite support interval (i.e., they are bounded), and the distributions $f(x, t_p, m_i)$ should be similarly bounded to avoid non-zero probabilities of unphysical values. For example, Tx90p is constrained to the range [0, 100], and precipitation-based hazard variables are often confined to the range [0, ∞). In these cases, the distributions should be truncated and renormalized by first integrating $f(x, t_p, m_i)$ to get the cumulative distribution function $F(x, t_p, m_i)$. If the support of the hazard x is given by [a, b], the truncated and renormalized PDF is then given by

$$f_{tr}(x, t_p, m_i) = \frac{f(x, t_p, m_i)}{F(b, t_p, m_i) - F(a, t_p, m_i)} \tag{2}$$

For any model and any projected time, we then have a most-likely value μ for Tx90p at that time, which represents the climate-driven signal, and a variance σ^2 that represents the natural variability around that value that is intrinsic to that model (Fig. 3). As noted above, the residuals for Tx90p from all the models are normally distributed. With the two values (μ and σ), Eq. (1) provides a normal distribution that represents the probability of the hazard for that model at that time (Fig. 4).

We now want to incorporate the uncertainty due to the differences among the different models (i.e., model spread) into our probabilistic projections. For any specified projection time t_p, we have 21 (possibly truncated) distributions $f(x, t_p, m_i)$ of Tx90p, each with a most-likely value and an associated variance (Fig. 5). We can use Eq. (3) to amalgamate the 21 normal distributions into a single finite mixture probability density function (Fig. 6),

$$f_{\text{mixture}}(x, t_p) = \sum_{i=1}^{N} w_i \, f(x, t_p, m_i) \tag{3}$$

where N is the number of models, x comprises values within the support interval of the hazard values, and w_i can be used to weight each model relative to the others. Weighting of the models could be performed if deemed supportable, but caution should be exercised as more information may be lost by inappropriate weighting than could potentially be gained by optimum weighting (e.g., Weigel et al., 2010). Here we assume that each model projection is equally valid, and we set $w_i = \mathrm{N}^{-1}$ for all i. The expected value for the hazard x at time t_p can be easily derived using

$$E(X, t_p) = \int_S x \, f_{\text{mixture}}(x, t_p) \, dx \tag{4}$$

where S is the support of X.

https://doi.org/10.5194/egusphere-2022-9
Preprint. Discussion started: 1 March 2022

Note that there is no expectation of normality in the mixture distributions provided by Eq. (3) and shown in Fig. 6, as there is no expectation that the model spread is normal or follows any other standard distribution type. There could be cases of outlier models for some hazard variable and/or location, which would tend to fatten the tails and/or introduce skewness, or there could be spread and clustering of models, which could create a bi- or multi-modal distribution. In our case of having a limited number of models, it would be challenging to determine whether the shape of the mixture distribution, particularly in cases of outlier models or multi-modal distributions with gaps between peaks, is a consequence of this limited sample or represents systematic differences between the physical constructs of the models. This is a necessary limitation that should be considered when interpreting these results.

With the N-model mixture distribution $f_{\text{mixture}}(x, t_p)$ provided by Eq. (3), which represents all the individual model probabilities as well as the spread between the models, we can easily integrate to obtain an exceedance probability curve (Fig. 6) that can be used to quantify various measures. The hazard distribution can also be linked directly to an impact/damage function to estimate risk/probability of loss. This will be explored further in Sect. 3.3.

Rather than establishing hazard exceedance probability in an individual year, it is often of interest to determine hazard exceedance probability over some time horizon or within some time period. This is generally referred to as the occurrence exceedance probability (OEP), which is the probability of exceeding some threshold at least once over multiple events. Our method as described here uses inter-annual variability and most-likely annual value, which provides an exceedance probability for any single year. In our case then, a year represents a single event. To find the likelihood of exceeding some hazard probability threshold in at least one year within some period of N years, the probabilities from each year are combined using the binomial distribution-derived formula to get the OEP for the random hazard variable X as

$$\text{OEP}(X) = 1 - \prod_{t=t_1}^{t_2}[1 - P_e(X, t)], \tag{5}$$

where t_1 and t_2 are the start and end times of the period of interest, and $P_e(X, t)$ is the hazard exceedance probability for each single year t between t_1 and t_2. For example, for the 30-year time horizon 2021–2050, the OEP curves of Tx90p in Palo Alto, CA USA following RCP4.5 and RCP8.5 are shown in Fig. 7.

3.2 Hazard probability (100-year fluvial flood)

Here we apply a method (AECOM, 2013) for estimating riverine discharge rates associated with the local 100-yr and 10-yr flood ($Q_{1\%}$ and $Q_{10\%}$ respectively). The method, described in more detail in Appendix C, is based on application of regression equations with three climate variables: the annual number of frost days (FD), the annual maximum number of consecutive dry days (CDD), and the annual-maximum 5-day precipitation (R5d). All three of these variables can be easily derived from the

https://doi.org/10.5194/egusphere-2022-9
Preprint. Discussion started: 1 March 2022

NEX-GDDP temperature and precipitation data. Discharge rates $Q_{1\%}$ and $Q_{10\%}$, in units of cubic feet per second (cfs), can be calculated from historical values of FD, CDD, and R5d in some specified baseline period, and from projected values following a specified emissions scenario. Recall that the climate variables FD, CDD, and R5d comprise annual time series, and thus $Q_{1\%}$ and $Q_{10\%}$ do as well. Our goal here is to estimate future changes in $Q_{1\%}$ and $Q_{10\%}$, and ultimately changes in return period of the historical 100-yr flood. In this case, the intrinsic variability of the models on inter-annual timescales is not as relevant as decadal or multidecadal variability. For example, we do not expect the return period of the historical 100-yr to vary from year to year in a meaningful way, but we may expect it to vary meaningfully from decade to decade. To remove inter-annual variability from the time series, we apply a moving window filter, so that the intrinsic variability of the models is constrained to longer timescales.

Note that when a hazard is a function of multiple climate variables, it is important to analyze the variance of the hazard and not the variance of the climate variables independently. For example, for any given model, there is no assumption that the variances of the three variables FD, CDD, and R5d, or more specifically, the variances of the residuals from the best-fit curves, are not correlated. It is likely that years with an anomalously small number of consecutive dry days may also be years with anomalously large maximum 5-day precipitation, and vice versa. That is, there is likely to be covariance between these three variables such that the variance of one variable is constrained by the variances of the other two. When the raw values for the climate variables are input into a model that estimates the hazard of interest, the covariance of the input variables is carried automatically through the model.

With values for historical $Q_{1\%}$ ($hQ_{1\%}$) and the projected (and smoothed) time series for $Q_{1\%}$ and $Q_{10\%}$ ($pQ_{1\%}$ and $pQ_{10\%}$), the change in return period of the historical 100-yr flood can be calculated using

$$x = \frac{hQ_{1\%} + pQ_{1\%} - 2pQ_{10\%}}{pQ_{1\%} - pQ_{10\%}} \quad (6)$$

where, assuming a logarithmic relationship between Q and return period RP, the historical 100-yr return period is given by $RP = 10^x$ (see Appendix C). Note that if there is no change in the projected 100-yr discharge (i.e., $pQ_{1\%} = hQ_{1\%}$), RP remains constant at 100 years as expected. As a cautionary note, Eq. (6) can become pathological if $pQ_{1\%} = pQ_{10\%}$, which, although neither physical nor likely, is still possible since $Q_{1\%}$ and $Q_{10\%}$ are calculated using two distinct regression expressions (Appendix C).

Time series of the exponent x and the probability of the projected return period of the historical 100-yr flood at a location in New Jersey, USA are shown in Fig. 8. In this example, by the 2020s, the expected value [as calculated with Eq. (4)] of the return period for the historical 100-yr flood has decreased to 46 years, and to 15 years by the 2090s.

https://doi.org/10.5194/egusphere-2022-9
Preprint. Discussion started: 1 March 2022

3.3 Risk / probability of loss

As a simple example of determining loss probability from hazard probability, a hypothetical asset in Palo Alto, CA USA may experience total loss in a year with Tx90p exceeding 40 (i.e., when the climatological warmest 10% temperatures are occurring 40% of the time) if no adaptation plan is in place to build climate resilience. In this case, we can use the hazard exceedance probabilities shown in Fig. 7 directly to determine the probability of ruin for the 30-year time horizon 2012–2050 (here we are considering a multi-year period and associated OEP, but the methodology can also be applied to the probability in a single year). In this highly simplified example, the probability of ruin over the 30-year period is 65% following RCP8.5 and about 27% following RCP4.5.

A broader description of loss probability can be derived from Tx90p hazard probability with the application of an impact function that links hazard to loss. To demonstrate this, we form a hypothetical impact function defined by

$$Y = \begin{cases} 0, \text{ if } 0 \le X \le 20 \\ \frac{1}{65}(X - 20), \text{ if } 20 \le X \le 85 \\ 1, \text{ if } 85 \le X \le 100 \end{cases} \quad (7)$$

where X is a random variable of hazard values x. Eq. (7) is also described visually in Fig. 9. There are several methods that can be used to deduce the probability of $Y = g(X)$ given the probability of X. Here we use inverse transform sampling to form a random variable X representing Tx90p. To form a random variable of loss values Y, we simply apply Eq. (7) with the elements x of the random variable X as input, and from the loss sample Y we can easily get the probability of loss exceedance curves shown in Fig. 10.

The loss exceedance probability curves shown in Fig. 10 can be used to form a wide variety of actionable information. For example, the maximum loss, with 95% confidence, can be found simply by identifying the intersect points of the curves with the 5% exceedance probability line (dashed line in Fig. 10). In this example, there is a 95% probability that loss will not exceed 37% (42%) in any year within the 30-year time horizon following RCP4.5 (RCP8.5). These loss values are typically referred to as the Value at Risk (VaR) with 95% confidence (e.g., Linsmeier and Pearson, 1996). Many other measures of risk can be deduced directly from these loss exceedance probability curves (e.g., Longerstaey, 1996).

4 Summary and discussion

We described a method to estimate projected hazards probabilistically. The projections are provided by a model ensemble. The probabilities are based on two distinct sources of uncertainty: 1) an estimate of the natural variability intrinsic to each model and 2) the differences among the models. Natural variability is estimated by separating the climate signal, which is

https://doi.org/10.5194/egusphere-2022-9
Preprint. Discussion started: 1 March 2022

described by a best-fit curve to each model time series, and then calculating the variance of the residuals from the best-fit curve. This provides a probability density function for each model at any projected time. The difference among the models is incorporated by forming a mixture distribution from the distributions of each model [Eq. (3)], from which a hazard exceedance probability curve is easily derived. There is a hazard exceedance curve for every projected time, and these can be combined into a hazard exceedance probability curve for any specified time horizon or interstitial time period [Eq. (5)]. Loss exceedance probability can be derived from the hazard exceedance probability via inverse transform sampling from the hazard exceedance probability curve and inputting the resulting sample directly into an impact function [e.g., Eq. (7)].

The method is applicable to any climate hazard time series provided with any temporal resolution (e.g., daily, monthly, annual, decadal, etc). The variance of the residuals from the most-likely values simply represents the intrinsic natural variability at whatever time resolution the data are provided at. In the case that the data are provided at daily temporal resolution, but the variability of interest occurs at longer time scales, then a low-pass smoother can be applied before fitting the time series to a best-fit curve and analyzing the residuals from that curve.

https://doi.org/10.5194/egusphere-2022-9
Preprint. Discussion started: 1 March 2022

Appendix A. Fitting model residuals to parametric distributions

For hazards for which the residuals from the quadratic best-fit curves are normally distributed, the two-parameter probability density function at any projected time can be constructed using Eq. (1) with the expected value (found along the best-fit curve at that time) and the standard deviation of the residuals for some model. For some hazards, however, the residuals are not normally distributed. This should be tested on a hazard-by-hazard basis to determine the optimal distribution to use. There are several ways to accomplish this. For our chosen method to determine this for any hazard variable, we choose a large sample of locations, calculate the residuals of the hazard time series at every location and model, fit those residuals to various parametric distributions, and choose the distribution that has the best goodness-of-fit as calculated by the mean of the Bayesian and Akaike Information Criteria at the locations. For the various temperature- and precipitation-based hazards that we have considered, we find that for hazards with non-normal residuals, a three-parameter generalized extreme value (GEV) distribution is often a good choice. We further find that the GEV distribution provides a comparatively much better goodness-of-fit to normally distributed residuals than a Gaussian fit provides for GEV-distributed residuals, due to the additional fitting parameter. In this case, if only one distribution were to be applied to all hazards, the GEV distribution is likely a better choice.

To apply the GEV distribution, the residuals from the best-fit curve for each model and location are analyzed to estimate the location, scale, and shape parameters (μ, σ, and ξ respectively). This is performed with the usual maximum likelihood estimation techniques. Once the location parameter μ is estimated from the residuals, it is shifted by an amount given by the value on the best-fit curve for any specified time, and the PDF of the hazard is given by

$$f(x, t_p, m_i) = \frac{1}{\sigma(m_i)} U(x, t_p, m_i)^{\xi(m_i)+1} \, e^{-U(x,t_p,m_i)}$$

where

$$U(x, t_p, m_i) = \begin{cases} \left(1 + \left(\frac{\left(x - \mu_{\text{shifted}}(t_p, m_i)\right)}{\sigma(m_i)}\right)\xi(m_i)\right)^{-1/\xi(m_i)} & \xi(m_i) \neq 0 \\ e^{\left(-\frac{x-\mu_{\text{shifted}}(t_p,m_i)}{\sigma(m_i)}\right)} & \xi(m_i) = 0 \end{cases}$$

Note that σ and ξ are functions of each model m_i but are constant in time, while μ_{shifted} is a function of model and time t_p because it relies on the values along the best-fit curve.

https://doi.org/10.5194/egusphere-2022-9
Preprint. Discussion started: 1 March 2022

Appendix B. Testing the assumption of stationary variance of the downscaled climate variables

The fundamental variables in the NEX-GDDP data, from which other hazard variables (e.g., Tx90p, annual maximum consecutive dry days, annual 5-day maximum precipitation, etc.) are derived, are based on daily maximum and minimum temperature and mean daily precipitation rate. If the variance of these basic variables is stationary, then the variables derived from them are assumed to have stationary variance as well. Here we use daily maximum temperature and mean daily precipitation rate at 45 locations globally to construct annual time series and test their variance for stationarity. The locations comprise a 5 x 9 grid with 40° spacing from 80°S to 80°N and from 0° to 320°E. For each model and for each location, annual-mean temperature and precipitation time series are derived from daily data, and then fit to a quadratic best-fit curve. The variance of the residuals from the first and second halves of the time series (2006–2099) are then compared (Figs. B1 and B2). We find that the changes in variance between the early and late periods for both temperature and precipitation behave essentially randomly with no clear systematic trend or bias, which supports the assumption of fixed variance.

Appendix C. Projected return period of the historical 100-yr riverine flood

The regression equations for the 100- and 10-year riverine discharge rates are described in detail in AECOM (2013) and are summarized here for convenience. They are given, respectively, by

$$Q_{1\%} = 1.321\ [DA^{0.711}\ SL^{0.169}\ (ST+1)^{-0.332}\ (IA+1)^{0.188}\ (FD+1)^{-0.206}\ (CDD+1)^{-0.177}\ (R5d+1)^{1.440}]$$
$$Q_{10\%} = 0.1093\ [DA^{0.723}\ SL^{0.158}\ (ST+1)^{-0.339}\ (IA+1)^{0.222}\ (FD+1)^{-0.044}\ (CDD+1)^{-0.395}\ (R5d+1)^{1.812}],$$

where DA is the drainage area of the watershed, in square miles, SL is the channel slope, in feet per mile, ST is the storage in the watershed as represented by the area of lakes and ponds, in percent of the drainage area, IA is the impervious area, in percent of the drainage area, FD is the annual number of frost days (minimum daily temperature ≤ 0°C), CDD is the annual maximum number of consecutive dry days (daily precipitation ≤ 1mm), and R5d is the annual maximum 5-day precipitation in mm. The four topographic variables DA, SL, ST, and IA are extracted from the HydroBasins dataset (Lehner and Grill, 2013). A graphical depiction of the derivation of Eq. (6) from the historical and projected values of $Q_{1\%}$ and $Q_{10\%}$ is shown in Fig. C1.

https://doi.org/10.5194/egusphere-2022-9
Preprint. Discussion started: 1 March 2022

Author contribution. JK, TH, and TT designed the experiments. JK developed the model code and performed the simulations. JK prepared the manuscript with contributions from TH and TT.

Competing interests. The authors declare that they have no conflict of interest.

References

AECOM, The impact of climate change and population growth on the National Flood Insurance Program through 2100, 2013.

Keenan, J. M.: A climate intelligence arms race, Science, 365, 1240–1243, doi:10.1126/science.aay8442, 2019.

Knutson, T. R., Zeng, F., Wittenberg, A. T., Multimodel assessment of regional surface temperature trends: CMIP3 and CMIP5 twentieth-century simulations, J. Clim., 26, 8709–8743, 2013.

Lehner, B., Grill G., Global river hydrography and network routing: baseline data and new approaches to study the world's large river systems. Hydrological Processes, 27(15): 2171–2186, 2013. Data is available at www.hydrosheds.org

Linsmeier, T. J., Pearson, N. D., Risk Management. An Introduction to Value at Risk. Working paper. University of Illinois at Urbana-Champaign, 1996.

Longerstaey, J., Risk Metrics—Technical Document. J.P. Morgan/Reuters, New York, 1996.

TCFD, Recommendations of the Task Force on Climate-related Financial Disclosures, Task Force on Climate-related Financial Disclosures, Financial Stability Board, Basel, Switzerland, 2017

TCFD, 2020 Status Report, Task Force on Climate-related Financial Disclosures, Financial Stability Board, Basel, Switzerland, 2020.

TCFD, 2021 Status Report, Task Force on Climate-related Financial Disclosures, Financial Stability Board, Basel, Switzerland, 2021.

Thrasher, B., Maurer, E. P., McKellar, C., Duffy, P. B., Technical Note: Bias correcting climate model simulated daily temperature extremes with quantile mapping. Hydrology and Earth System Sciences, 16, 3309-3314, doi:10.5194/hess-16-3309-2012, 2012.

Venables, W. N., Ripley, B. D., Modern Applied Statistics with S. Fourth Edition. Springer, New York. ISBN 0-387-95457-0, 2002.

Weigel, A. P., Knutti, R., Liniger, M. A., Appenzeller, C., Risks of Model Weighting in Multimodel Climate Projections, J. Clim., 26, 4175–4191, 2010

https://doi.org/10.5194/egusphere-2022-9
Preprint. Discussion started: 1 March 2022

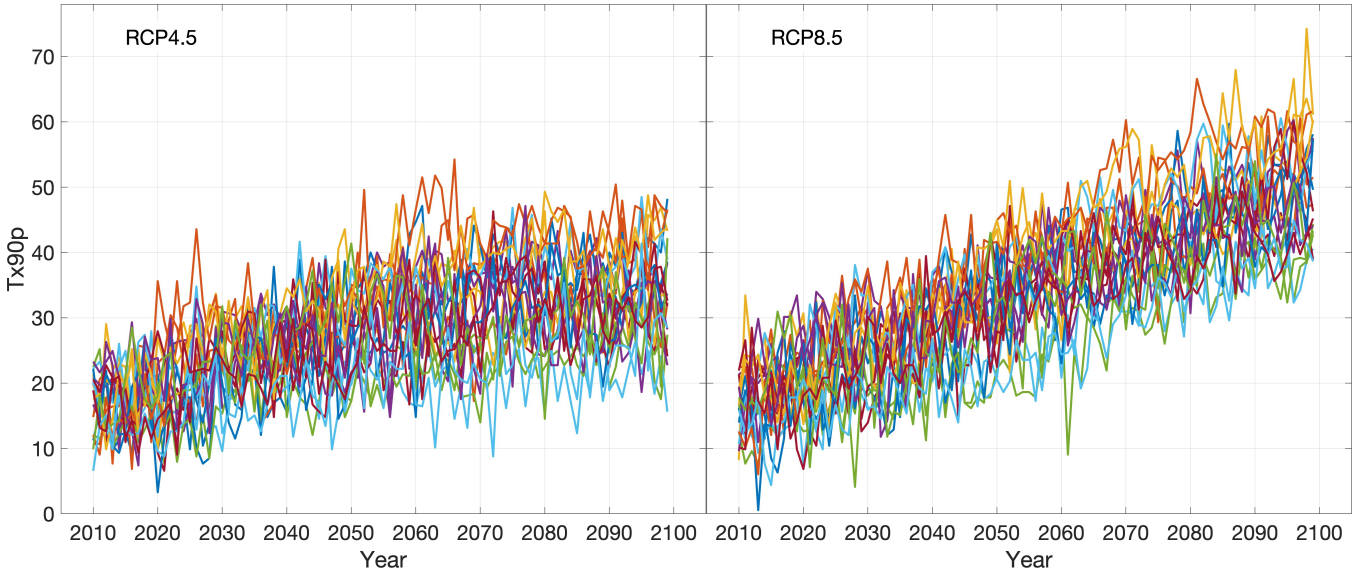

Figure 1: Time series of Tx90p in Palo Alto, CA USA downscaled from 21 CMIP5 models under RCP4.5 and RCP8.5.

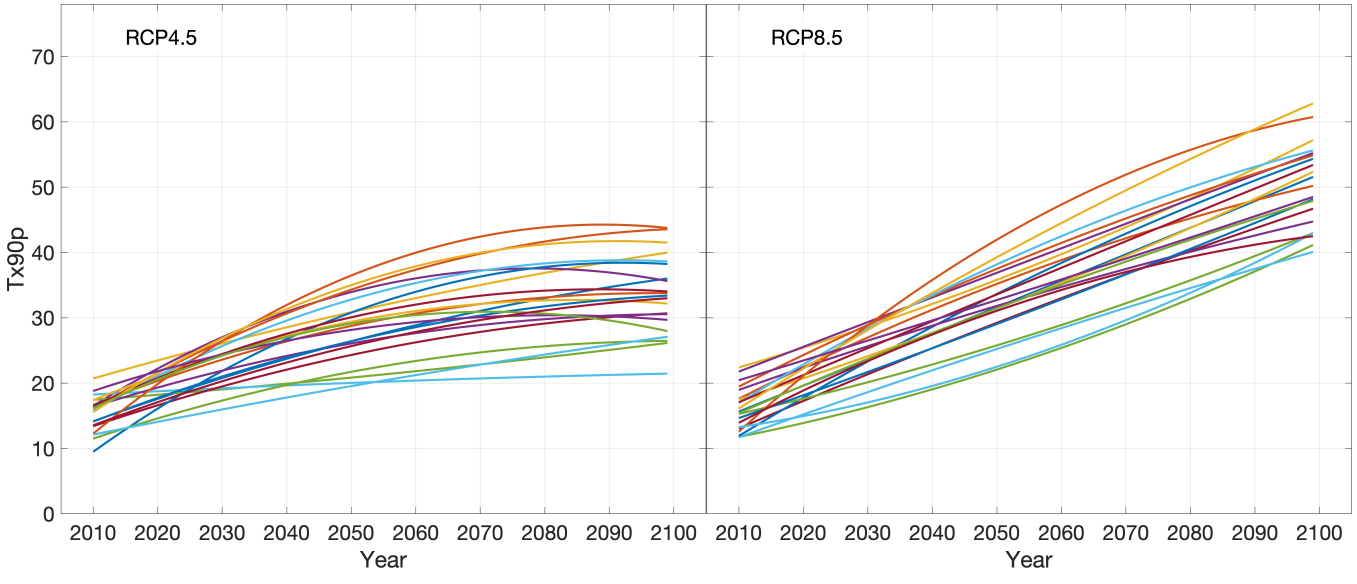

Figure 2: Quadratic best-fit curves fit to the time series in Figure 1.

https://doi.org/10.5194/egusphere-2022-9
Preprint. Discussion started: 1 March 2022

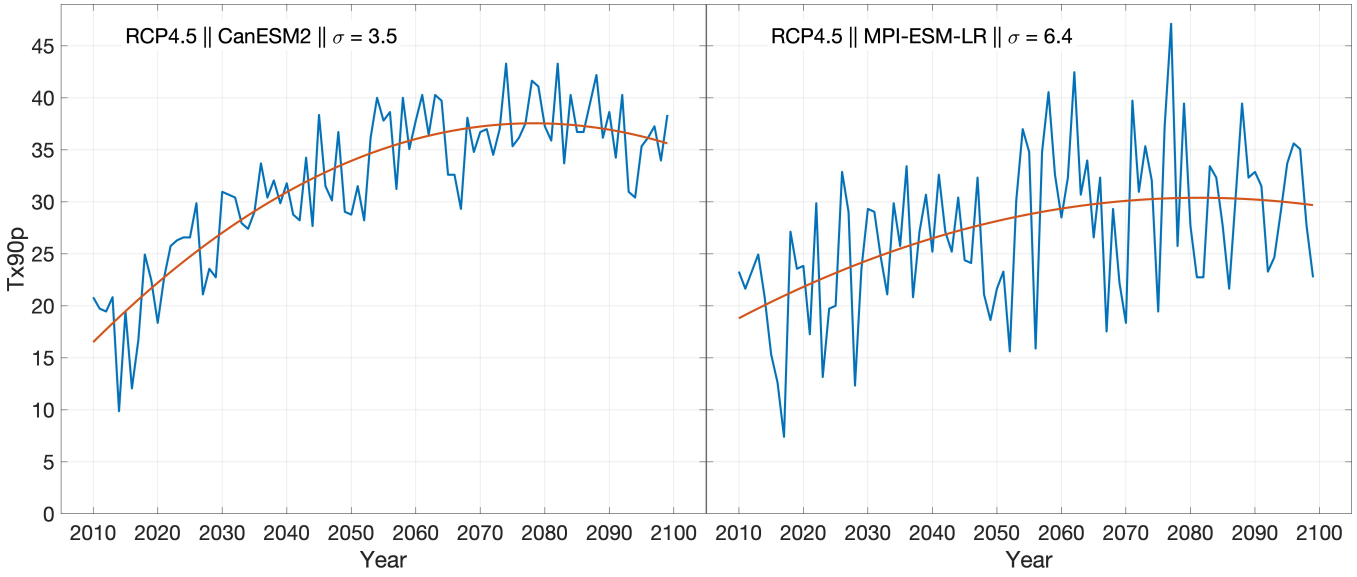

Figure 3: Time series of Tx90p in Palo Alto, CA USA downscaled from 2 of the 21 CMIP5 models under RCP4.5. The CanESM2 model exhibits the smallest amplitude natural variability of the 21 models, and the MPI-ESM-LR model exhibits the greatest amplitude natural variability. The standard deviations (σ) of the residuals from the best-fit curves (red) are shown. The differences in the best-fit curves demonstrate the differences in how each model represents the climate-change signal.

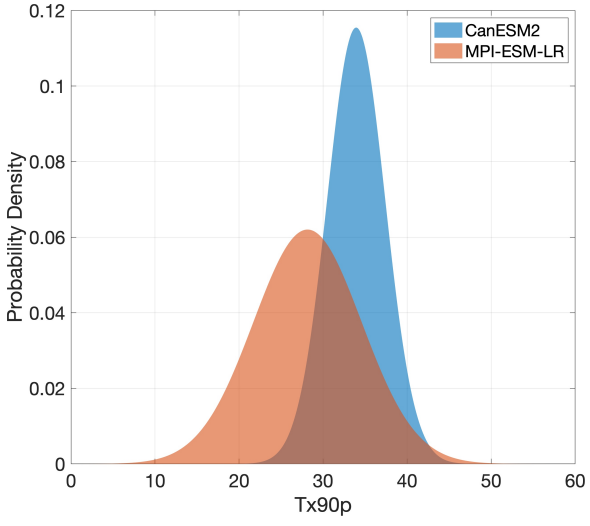

Figure 4: Projected normal distributions of Tx90p in the year 2050 for the two models described in Figure 3.

https://doi.org/10.5194/egusphere-2022-9
Preprint. Discussion started: 1 March 2022

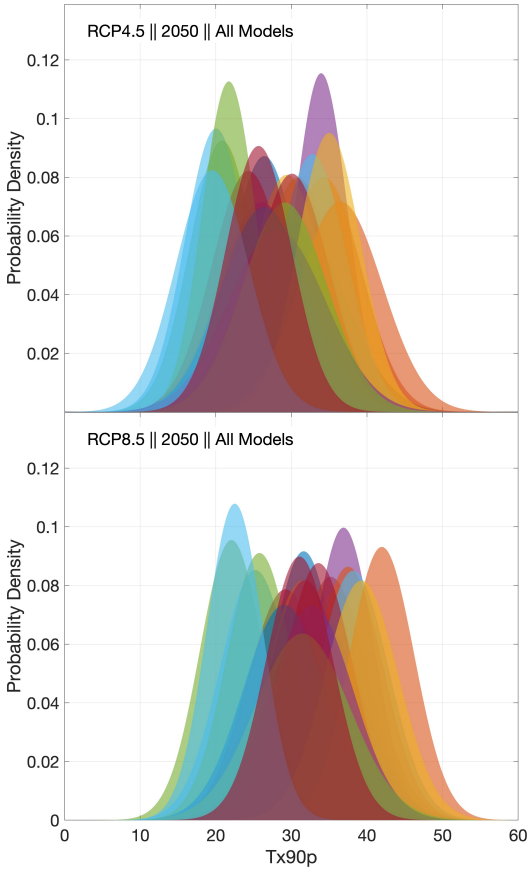

Figure 5: Projected normal distributions of Tx90p in the year 2050 for 21 CMIP5 models under RCP4.5 and RCP8.5.

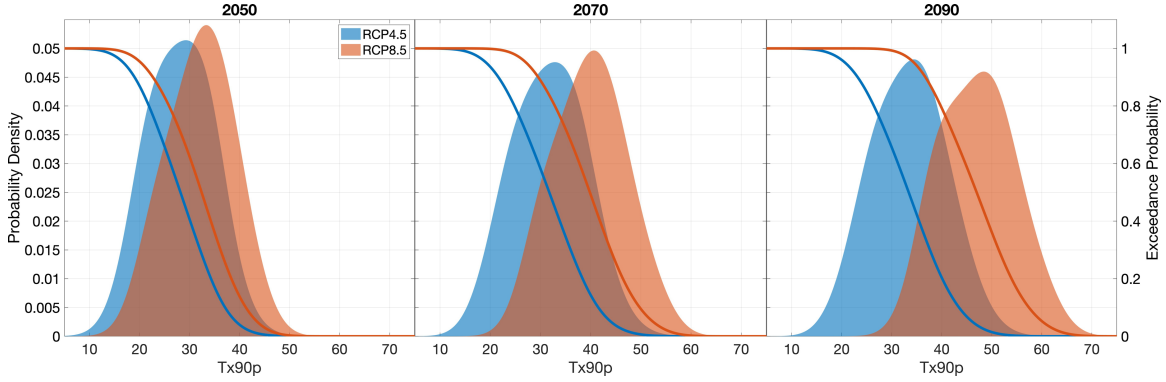

Figure 6: Amalgamated distributions (finite mixture distributions) in the year 2050 (left panel) at Palo Alto, CA USA following RCP4.5 (blue shading) and RCP8.5 (red shading). These probability density distributions (scaled on the left axis) represent both sources of uncertainty; from each of the 21 model's intrinsic natural variability, and from the spread between the 21 models. Also shown are the associated exceedance probability curves (scaled by the right axis). To demonstrate the projected time-evolution of the hazard probability, the middle and right panels also show the distributions and exceedance probability curves for the years 2070 and 2090, respectively.

https://doi.org/10.5194/egusphere-2022-9
Preprint. Discussion started: 1 March 2022

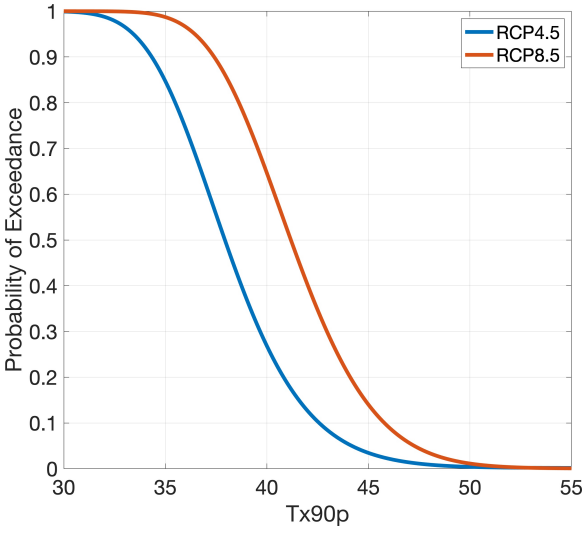

Figure 7: Occurrence exceedance probability of the hazard following RCP4.5 (blue) and RCP8.5 (red). The probability is calculated using Eq. (5) over a 30-year time horizon with t_1 = 2021 and t_2 = 2050.

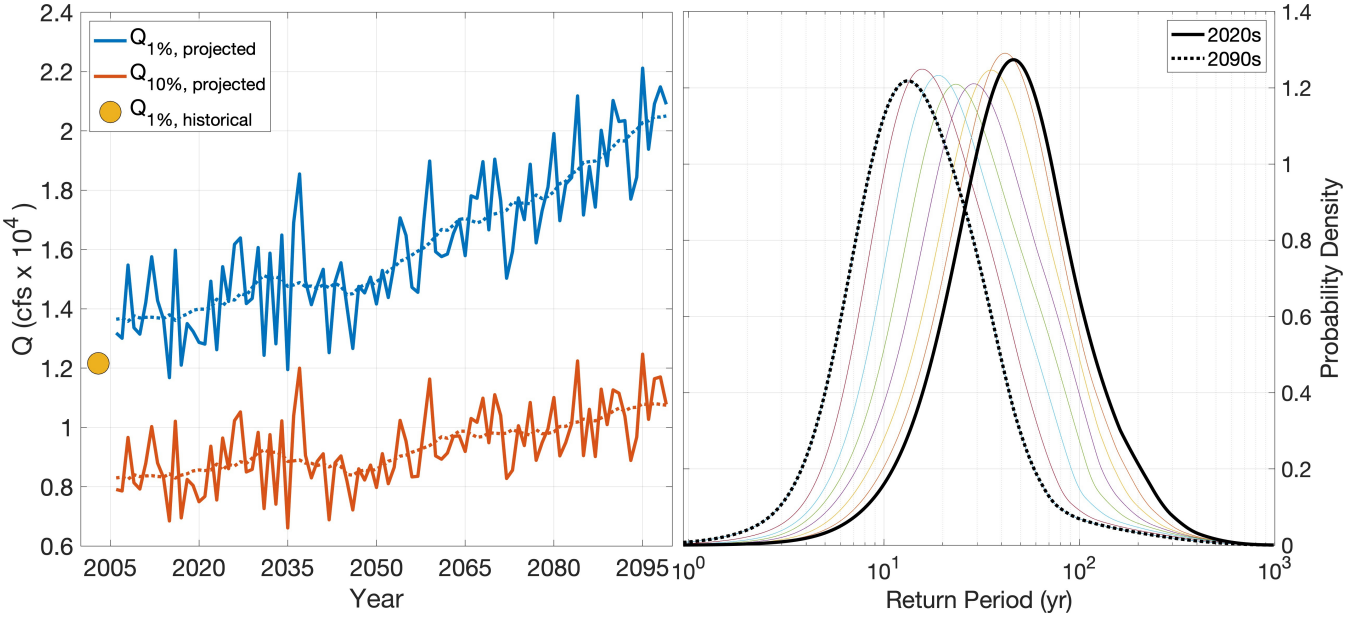

Figure 8: Left panel: Time series of projected riverine discharge rates for the 100-yr (blue) and 10-yr (red) flood. Solid curves show the raw annual time series, dotted lines show the low-pass-filtered time series, and the yellow marker shows the historical 100-yr flood discharge rate (for the period 1950–1999). The projections follow the RCP8.5 scenario, and the location is in New Jersey, USA. Right panel: Evolution of the probability of the return period of the historical 100-yr flood (colored curves) from the 2020s (solid black curve) to the 2090s (dashed black curve).

https://doi.org/10.5194/egusphere-2022-9
Preprint. Discussion started: 1 March 2022

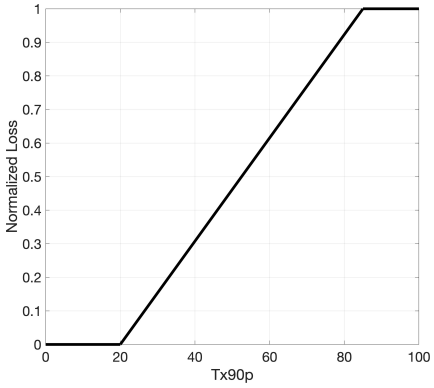

Figure 9: Hypothetical impact function relating loss to hazard (Tx90p). Loss is normalized to the interval [0, 1]. Loss is zero until Tx90p = 20 and then increases linearly with hazard until Tx90p = 85, beyond which total loss occurs.

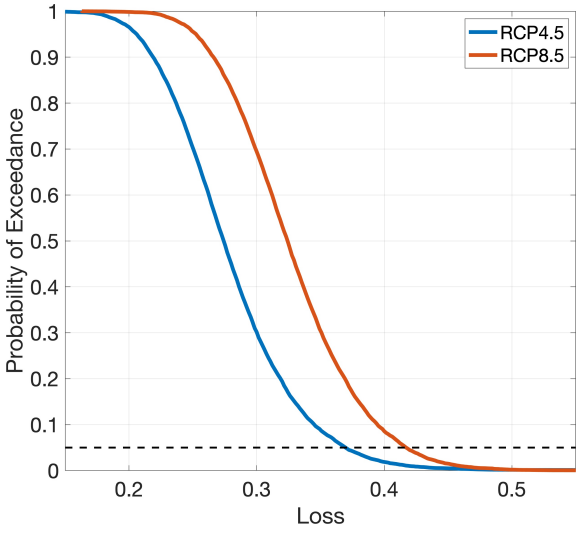

Figure 10: Occurrence exceedance probability of loss following RCP4.5 (blue) and RCP8.5 (red) over the 30-year period 2021–2050. In this example, there is 95% confidence that loss will not exceed 37% (42%) in any year within the 30-year time horizon following RCP4.5 (RCP8.5).

https://doi.org/10.5194/egusphere-2022-9
Preprint. Discussion started: 1 March 2022

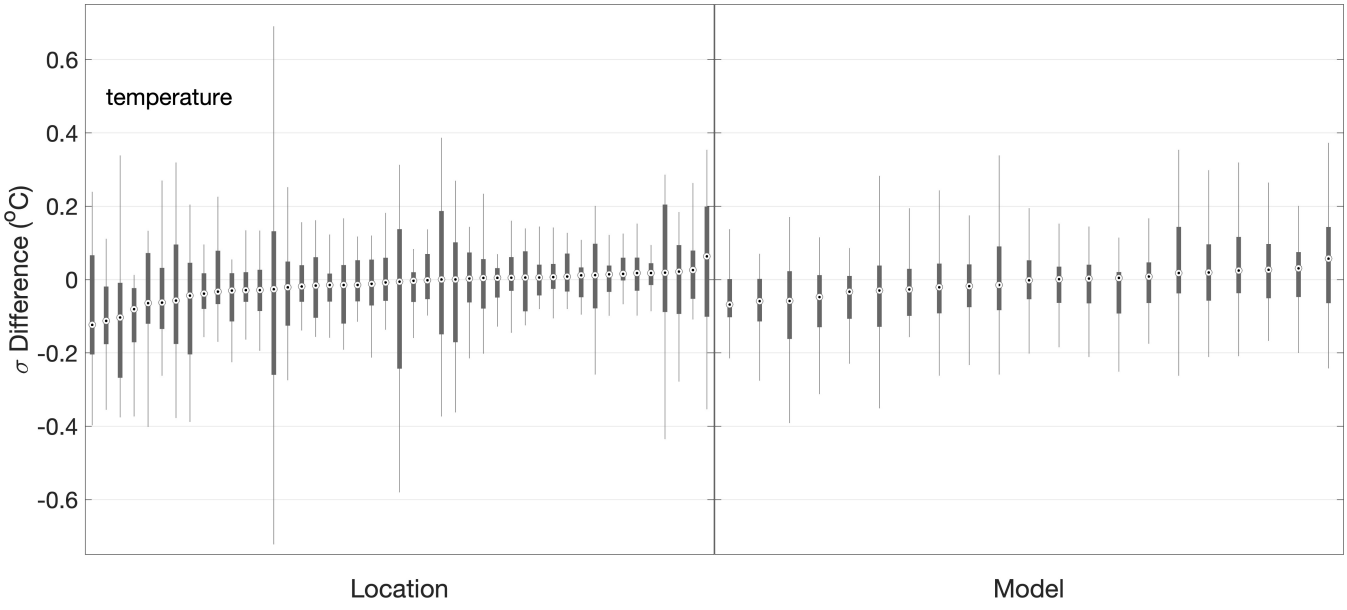

Figure B1: Box and whiskers plots showing the difference in standard deviation in the daily-maximum-temperature time series between the first and second halves of the period 2006–2099. Difference among the 21 models at the 45 global locations (left) and among the 45 locations for each model (right). The interquartile ranges (shaded grey boxes) generally span zero, suggesting random variation rather than any systematic change over time. The boxes are sorted by their median values (open circles with dots) for display purposes.

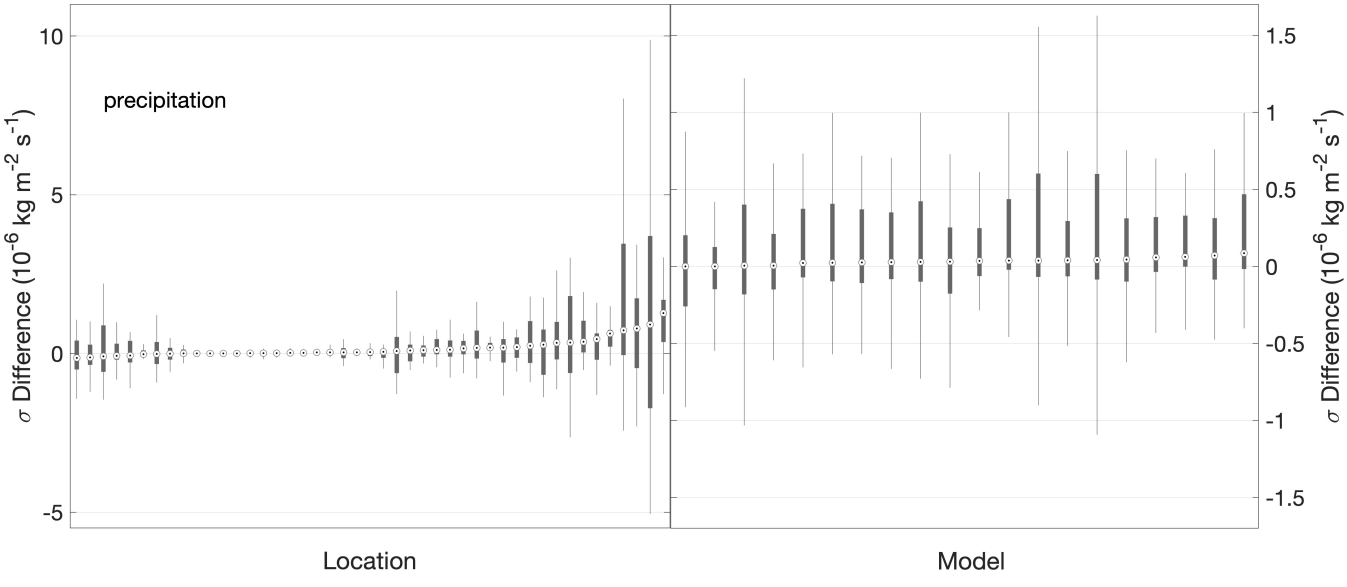

Figure B2: Similar to Fig. A1, but for daily maximum precipitation.

https://doi.org/10.5194/egusphere-2022-9
Preprint. Discussion started: 1 March 2022

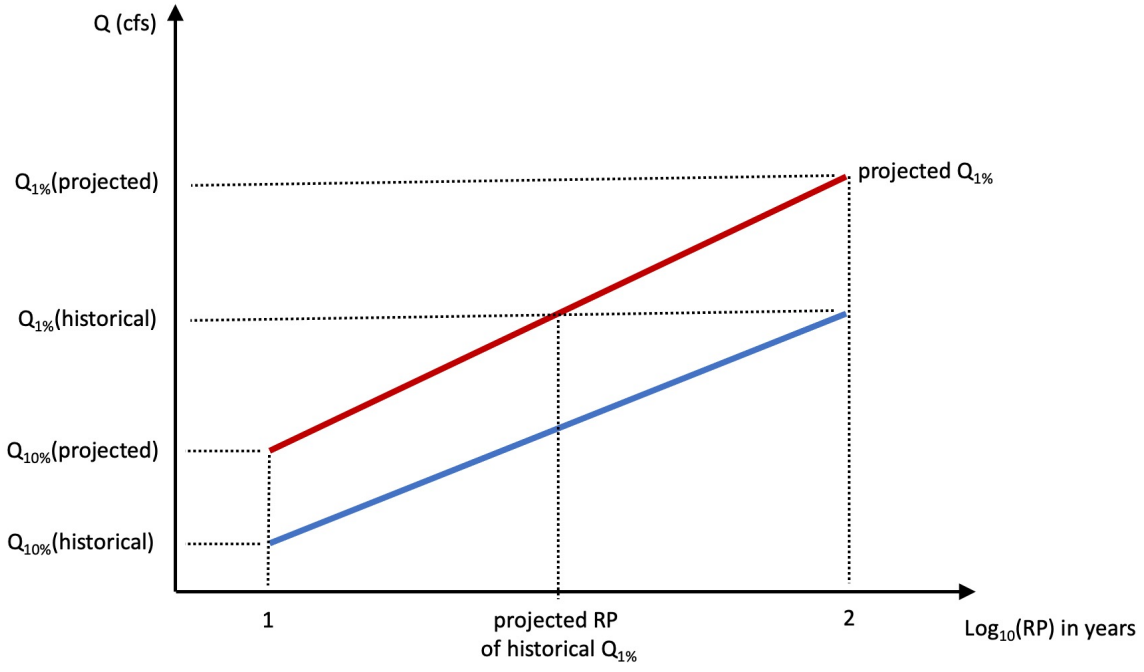

380 **Figure C1: Schematic showing the derivation of the projected return period (RP) of the historical 100-yr flood.**